Mechanical and Microstructural Performances of One-Part Alkali-Activated Fly Ash Mortars with Thermally Activated Palm Oil Decanter Cake

Yoon Tung Chan[1], Nor Hasanah Abdul Shukor Lim[2,*], Shafiq Ishak[2,*], Mostafa Samadi[3], Shek Poi Ngian[2], Hong Yee Kek[4] and Shea Qin Tan[1]

[1]*Faculty of Civil Engineering, University of Technology Malaysia (UTM), Johor Bahru, Johor 81310, Malaysia*

[2]*UTM Construction Research Center (CRC), Department of Structure and Materials, Faculty of Civil Engineering, University of Technology Malaysia (UTM), Johor Bahru, Johor 81310, Malaysia*

[3]*Institute of Energy Infrastructure, Universiti Tenaga Nasional, Jalan IKRAM-UNITEN, Kajang, 43000, Selangor, Malaysia*

[4]*School of the Built Environment, Universiti of Reading Malaysia, Johor, Malaysia*

Abstract: The utilisation of waste-derived precursors in one-part alkali-activated materials offers a promising route towards more sustainable cementitious systems. This study evaluates calcined palm oil decanter cake (PODC) as a partial replacement for Class C fly ash in one-part alkali-activated mortars. PODC was thermally treated at 400 °C to reduce organic content while retaining biochar and incorporated at replacement levels of 5–20%. Fresh properties, physical characteristics, mechanical performance, and microstructural development were systematically assessed. Increasing PODC content reduced flowability and shortened setting time, attributed to the lower density, irregular particle morphology, and water-retention behaviour of biochar. Despite these changes, bulk density, water absorption, and apparent porosity were only marginally affected, indicating that matrix compactness was largely preserved. Strength development depended strongly on replacement level. Mortars with 10% and 15% PODC showed improved performance relative to the control, with 15% achieving the highest long-term compressive strength due to additional reactive Ca, K, and Si contributed by PODC. The 10% replacement provided a more balanced response, combining improved workability, stable early-age strength, and enhanced flexural and splitting tensile strengths. In contrast, 20% replacement led to strength reduction associated with increased porosity and a weaker interfacial transition zone. XRD, TG–DTA, and SEM–EDS confirmed substantial consumption of PODC phases and the formation of well-developed binding gels (C–S–H, C–A–S–H, and alkali-substituted (N,K)–A–S–H). Residual biochar acted as a preferential site for gel nucleation, promoting matrix cohesion. Overall, calcined PODC is an effective supplementary precursor for one-part fly ash-based alkaline-activated mortars, with an optimal replacement range of 10–15%.

Keywords: One-part alkali-activation, Palm Oil Decanter Cake, Fly Ash, Mechanical, Microstructural.

1. INTRODUCTION

The construction industry is under increasing pressure to reduce its environmental footprint due to the high energy consumption and carbon emissions associated with ordinary Portland cement (OPC) production [1]. Alkali-activated materials (AAMs), particularly those based on industrial by-products such as fly ash and slag, have emerged as promising low-carbon alternatives owing to their reduced greenhouse gas emissions, superior durability, and flexible raw material sourcing [2]. Among these systems, one-part or “just-add-water” AAMs have gained growing attention because they overcome the handling, safety, and logistical challenges associated with conventional two-part alkali-activated binders that rely on liquid alkaline solutions [3].

Class C fly ash (FA) is widely used as a precursor in one-part AAMs due to its high calcium content, which promotes rapid strength development through the formation of calcium-rich binding gels such as C–S–H and C–A–S–H, alongside alkali aluminosilicate phases [4]. However, the availability and quality of FA are becoming increasingly uncertain due to the global transition away from coal-fired power generation [5]. This challenge has stimulated research into alternative supplementary precursors derived from industrial and agricultural waste streams, with the dual aim of ensuring long-term material supply and improving the sustainability of AAMs systems.

Palm oil decanter cake (PODC) is an abundant biomass residue generated during palm oil milling, particularly in Southeast Asia [6]. Large quantities of PODC are currently underutilised or disposed of through landfilling and open dumping, posing environmental concerns. Previous studies have shown that thermally treated biomass residues can serve as reactive or functional components in cementitious systems, either by contributing mineral phases or by acting as microstructural modifiers [7]. When calcined at moderate temperatures, PODC undergoes substantial organic decomposition while retaining a

*Address correspondence to this author at the UTM Construction Research Center (CRC), Department of Structure and Materials, Faculty of Civil Engineering, University of Technology Malaysia (UTM), Johor Bahru, Johor 81310, Malaysia; E-mail: norhasanah@utm.my; shafiq.ishak@utm.my

Received on 18-11-2025 Accepted on 26-12-2025 Published on 30-12-2025

E-ISSN: 2311-8717/25

biochar-rich fraction and inorganic oxides such as SiO_2, CaO, Al_2O_3, and K_2O [8]. These characteristics suggest that calcined PODC may be suitable for use as a supplementary precursor in alkali-activated binders.

Recent investigations into biochar-modified cementitious materials have reported mixed effects on fresh and hardened properties [9]. While biochar can enhance internal curing, crack resistance, and long-term durability through its porous structure and water-retention capacity, excessive biochar addition may increase porosity and weaken the interfacial transition zone (ITZ) [10]. In AAMs systems, the interaction between biochar, alkaline activators, and aluminosilicate precursors is further complicated by the coexistence of multiple binding gels and the sensitivity of alkali activation reactions to water availability and particle morphology [11]. Despite growing interest, systematic studies examining the role of calcined PODC in one-part alkali-activated fly ash mortars remain limited.

In particular, there is a lack of comprehensive understanding regarding the optimal replacement level of calcined PODC that balances fresh workability, mechanical performance, and microstructural development in one-part AAMs systems. Furthermore, the contribution of potassium-rich phases and residual biochar from calcined PODC to gel chemistry, strength development, and interfacial bonding in high-calcium FA systems has not been fully elucidated. Therefore, this study aims to investigate the feasibility of incorporating calcined palm oil decanter cake (PODC_Calcined) as a partial replacement for Class C FA in one-part AAMs mortars. PODC was incorporated at replacement levels ranging from 5% to 20%, and its effects on fresh properties, physical characteristics, mechanical performance, and microstructural evolution were systematically evaluated. Advanced characterisation techniques, including XRD, FTIR, TG–DTA, and SEM–EDS, were employed to elucidate reaction mechanisms and gel formation. The findings of this study provide new insights into the synergistic role of biochar-rich agricultural waste in one-part AAMs systems and demonstrate the potential of calcined PODC as a sustainable supplementary precursor for high-performance construction materials.

2. MATERIALS AND METHODS

2.1. Materials

The PODC utilised in this study was sourced from Ladang Alaf, Johor, Malaysia, while the Class C fly ash (FA) was obtained from a local supplier in Johor. Before being employed as the primary precursor, the FA was subjected to a series of characterisation tests. The oxide composition was determined using X-ray fluorescence (XRF) analysis and the results are summarised in Table **1**. The FA was found to contain 34.34% CaO and 22.45% SiO_2 as the major components, together with Fe_2O_3 (16.63%), MgO (11.04%), and Al_2O_3 (10.38%). The fly ash was categorised as Class C based on the chemical requirements specified in ASTM C618 [12]. The specific surface area (SSA) was determined through nitrogen (N_2) adsorption–desorption isotherms using the BET method, giving a value of 2.09 m²/g. The density of the FA measured using a helium (He) pycnometer was found to be 3.31 g/cm³.

Table 1: Material Properties of FA

Oxide Composition (%)	Fly Ash
SiO_2	20.69
CaO	31.65
Al_2O_3	9.57
Fe_2O_3	15.33
MgO	10.18
Others	4.77
L.O.I[a]	7.81
Sum	100.00
Specific surface area (m^2/g)	2.09
Density (g/cm^3)	3.31
D_{50} (μm)	9.04

The X-ray diffraction (XRD) pattern of the FA (Figure **1a**), obtained using a SmartLab diffractometer (Rigaku, Japan), confirms the presence of both amorphous and crystalline phases. Quartz and ferrite constitute the dominant crystalline phases, while periclase, portlandite, lime, and calcite appear as minor phases. Particle size distribution (PSD) is presented in Figure **1b,** where the median particle diameter (D_{50}) was recorded as 9.04 μm. Morphological analysis conducted via scanning electron microscopy is shown in Figure **1c,** revealing predominantly spherical particles with smooth surfaces, typical of Class C FA. Fourier transform infrared (FTIR) spectroscopy (Nicolet iS20, U.S.A.), shown in Figure **1d**, exhibits a distinct absorption band at 2361.80 cm^{-1} corresponding to CO_2, likely arising from the breakdown and reformation of carboxyl (C=O) and carbonyl (C–O–C) functionalities [13]. In the fingerprint region below 1500 cm^{-1}, the prominent peak at 1098.76 cm^{-1} is associated with Si(Al)–O–Si stretching vibrations characteristic of silicate glass structures [14]. While the band at 607.31 cm^{-1} reflects Si–O–Al stretching, confirming the presence of aluminosilicate phases [15].

The freshly collected PODC from the palm oil mill was initially received in a water-saturated condition. It was first oven-dried at 105 °C for 24 hours to eliminate

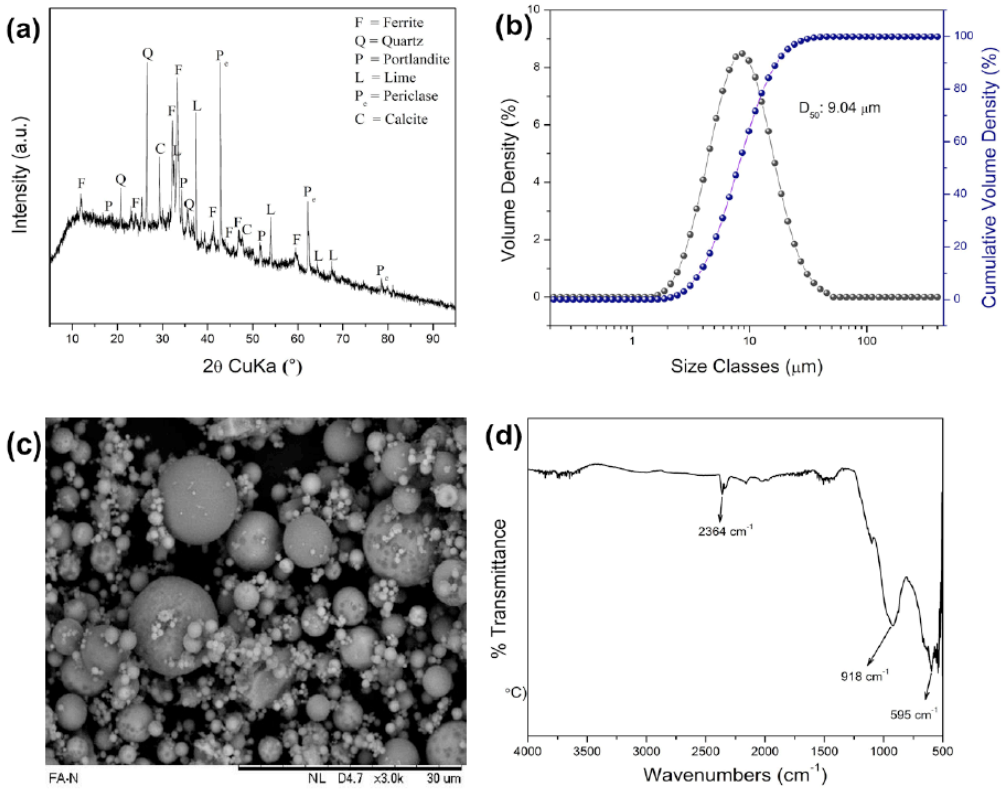

Figure 1: (**a**) XRD, (**b**) PSA, (**c**) micrograph, and (**d**) FTIR of FA

free moisture. Following drying, the material was milled at 30 rpm for 3 hours and subsequently sieved to obtain a powder fraction passing the 45 µm sieve, in accordance with ASTM C430 [16], Standard Test Method for Fineness of Hydraulic Cement by the 45-µm (No. 325) Sieve. The resulting PODC powder was then subjected to calcination in a muffle furnace at a target temperature of 400 °C for 2 hours. Figure **2a** presents the appearance of the calcined PODC, while Figure **2b** provides a magnified view illustrating the presence of residual biochar following the calcination process.

Table **2** presents the XRF and density results of the raw PODC and PODC calcined at 400 °C. The major oxides identified in both states include SiO_2, CaO, Al_2O_3, K_2O and Fe_2O_3. Following activation at 400 °C, the relative proportions of these oxides increase compared with the raw PODC. This increase is attributed to the loss of organic matter such as carbon, residual oil and moisture during thermal treatment, which reduces the total mass of the sample and consequently elevates the relative percentage of inorganic oxides [17]. The CHNS analysis shown in Table **3** corroborates this observation. The raw PODC contains a high carbon content of 33.6%, whereas calcination at 400 °C reduces the carbon content to 2.4%, with the remaining fraction present mainly in the form of biochar (Figure **2b**). This significant decline confirms the decomposition and volatilisation of organic constituents, consistent with the changes observed in the XRF profiles.

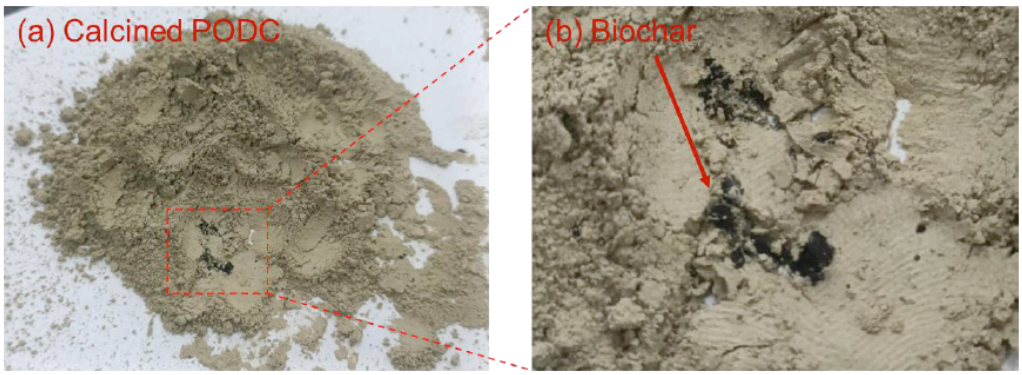

Figure 2: (**a**) Calcined PODC and (**b**) Biochar

Table 2: Oxides Analysis of Raw and Calcined PODC

Chemical Compounds	PODC_Raw	PODC_Calcined
SiO_2	13.98	40.21
CaO	3.11	11.49
Al_2O_3	1.96	10.59
K_2O	1.57	7.52
Fe_2O_3	1.29	5.11
Others	4.12	9.98
LOI	73.97	15.1
Density (g/cm^3)	1.95	2.81

Figure **3a** presents the XRD pattern of the replacement precursor, namely calcined PODC, used in the one-part AAMs system. The diffractogram indicates that the material is predominantly crystalline, with quartz identified as the major phase, accompanied by minor peaks corresponding to calcite and magnetite. Nevertheless, a discernible amorphous hump is observed in the range of 18–35°, suggesting the presence of residual amorphous phases that may contribute to alkali reactivity. Figure **3b** illustrates the PSD of the calcined PODC, where the mean particle size is recorded as 13.60 µm, satisfying the fineness requirement specified in ASTM C430 [16]. The microstructural features of the calcined PODC are shown in Figure **3c**. The SEM images reveal irregularly shaped particles together with rod-like porous structures, reflecting the structural transformation induced by thermal treatment. Figure **3d** shows the FTIR spectrum of the calcined PODC. Prominent absorption bands are observed at approximately 2386 cm^{-1}, 1408 cm^{-1}, and 1011 cm^{-1}. The band at 2386 cm^{-1} is attributed to CO_2, likely arising from the cracking and reformation of carboxyl (C=O) and carbonyl (C–O–C) functional groups [13]. The peak at 1408 cm^{-1} is associated with the deformation of cellulose and hemicellulose residues [18], while the absorption band at 1011 cm^{-1} corresponds to Si(Al)–O–Si stretching vibrations, characteristic of silicate glass structures [19].

Anhydrous sodium metasilicate (ASM), with a density of 1.17 g/cm³, was used as the alkaline

Table 3: CHNS Analysis of PODC

Chemical Compounds	Carbon (%)	Hydrogen (%)	Nitrogen (%)	Sulphur (%)
PODC_Raw	33.6	4.4	2.0	0.8
PODC_Calcined	2.4	0.4	0.4	1.1

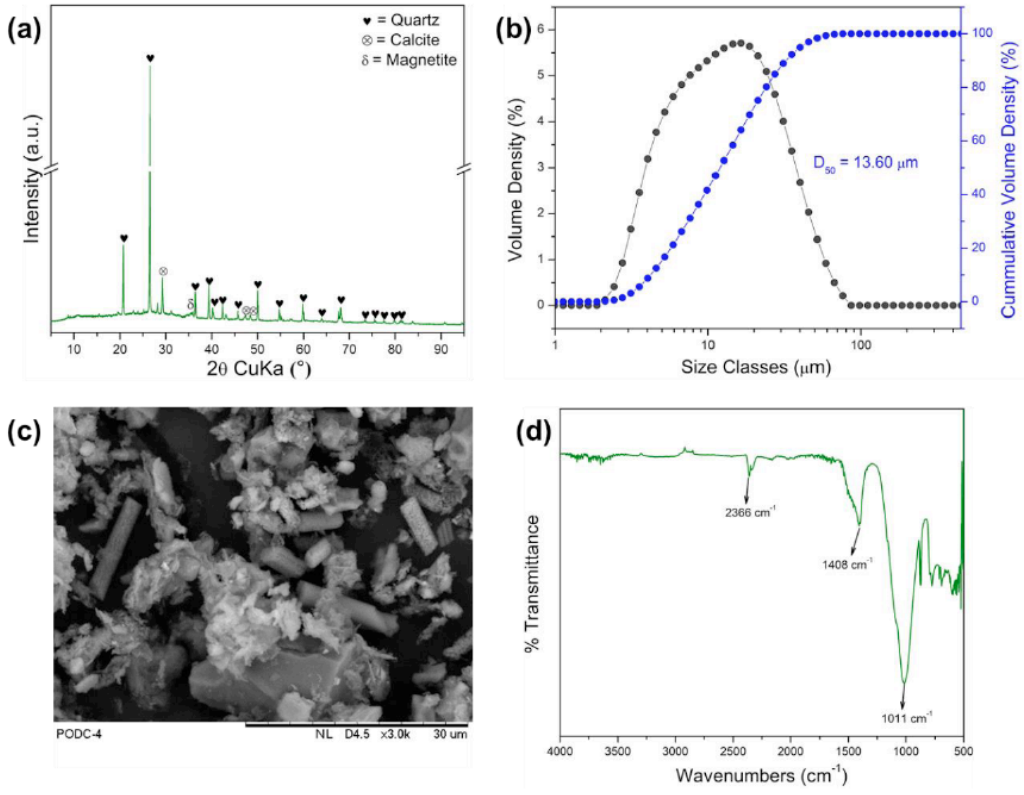

Figure 3: (**a**) XRD, (**b**) PSA, (**c**) micrograph, and (**d**) FTIR of PODC_Calcined.

activator in this study. The activator comprised Na_2O and SiO_2 contents of 50.8% and 46.97%, respectively, corresponding to a silicate modulus of 0.93. A polyacrylic-based superplasticiser was incorporated to improve the flowability of the fresh mortar. River sand sourced from a local supplier was used as the fine aggregate.

2.2. Mixing Process of Fly Ash-Based PODC Mortar

In this study, PODC_Calcined was incorporated at replacement levels of 5%, 10%, 15% and 20% to evaluate the effect of varying PODC contents on the performance of one-part alkali-activated FA systems. The selected replacement range was determined based on preliminary experimental investigations, which indicated that PODC incorporation beyond 20% resulted in a noticeable reduction in the mechanical performance of the AAMs mortars. The sand-to-binder, water-to-binder and superplasticiser-to-binder ratios were fixed at 1.5, 0.36 and 0.015, respectively. The dosage of the alkaline activator was maintained at 30% relative to the water content.

For sample preparation, FA, PODC and ASM were first dry-mixed manually until a uniform powder blend was obtained. The dry mixture was then mixed for 4 minutes using a Hobart mixer, during which water was added gradually. A polyacrylic-based superplasticiser was subsequently introduced to achieve the desired workability of the fresh paste. The fresh mortar was cast into 50 × 50 × 50 mm cube moulds and covered with plastic film to minimise moisture loss. After demoulding, the specimens were sealed in plastic zip-lock bags and stored until the designated testing ages. The detailed mix proportions are summarised in Table **4**. For microstructural characterisation, paste samples were prepared in conical tubes. Hydration was arrested using the solvent exchange method with isopropyl alcohol, following the procedure described by Snellings *et al*. [20].

2.3. Test Methods

2.3.1. Fresh Properties

The fresh-state behaviour of the mixtures was evaluated through setting time measurements on paste samples and flowability tests on mortar samples. The setting time was determined using the Vicat needle method in accordance with ASTM C191 [21], while the flowability of the mortar was assessed following ASTM C1437 [22].

2.3.2. Density, Absorption, and Voids Test

The density, water absorption and apparent void content of the hardened mortar specimens were evaluated following the procedures specified in ASTM C642 [23]. “Standard Test Method for Density, Absorption, and Voids in Hardened Concrete”.

2.3.3. Ultrasonic Pulse Velocity (UPV) test

Ultrasonic pulse velocity (UPV) measurements were performed on the mortar specimens in accordance with ASTM C597 [24]. “Standard Test Method for Ultrasonic Pulse Velocity Through Concrete” for mortar samples”.

2.3.4. Compressive Strength Test

Compressive strength testing was performed in accordance with ASTM C109 [25] using a universal testing machine (Eco Smartz Automatic Compression Machine, 3000 kN) at a loading rate of 0.9 kN/s. The reported compressive strength values represent the average of three specimens tested after curing periods of 1, 3, 7, 14, 28, 56 and 90 days.

2.3.5. Flexural Strength Test

Flexural strength testing was conducted in accordance with ASTM C348 [26] on mortar prisms with dimensions of 40 × 40 × 160 mm. The tests were performed using a universal testing machine similar to compressive strength test, equipped with a steel flexural loading frame to facilitate three-point bending. A constant loading rate of 0.05 kN/s was applied until failure. The reported flexural strength values represent the average of three specimens tested at a curing age of 28 days.

2.3.6. Splitting Tensile Strength Test

Splitting tensile strength testing was carried out following ASTM C496 [27] using cylindrical mortar specimens with dimensions of 50 × 100 mm. The tests

Table 4: Mix Proportion of Mortar Samples

Type of Sample	FA (kg/m^3)	PODC (kg/m^3)	ASM (kg/m^3)	Sand (kg/m^3)	Water (kg/m^3)	SP (kg/m^3)
FA_Activated	733	0	113.1	1100	264	11
FA_PODC_5%	696	37	113.1	1100	264	11
FA_PODC_10%	660	73	113.1	1100	264	11
FA_PODC_15%	623	110	113.1	1100	264	11
FA_PODC_20%	586	147	113.1	1100	264	11

were performed using the same universal testing machine as the compressive strength test, fitted with steel bearing strips to ensure uniform load distribution along the specimen diameter. A loading rate of 0.9 kN/s was applied continuously until specimen failure. The average splitting tensile strength of three specimens tested at a curing age of 28 days was reported.

2.3.7. X-Ray Diffraction (XRD)

The crystalline phases of the samples after 28 days of curing were characterised using XRD (SmartLab, Rigaku, Japan) with Cu Kα radiation (λ = 1.5405 Å). The diffractometer was operated at an accelerating voltage of 40 kV and a current of 30 mA. Data were collected over a 2θ range of 3–100° at a scanning rate of 8.2551°/min.

2.3.8. Thermogravimetric-Differential Thermal Analysis (TG-DTA)

The thermal behaviour and weight loss of the hydrated samples were analysed using a thermogravimetric–differential thermal analyser (DTG-60H, Shimadzu, Japan). The specimens were heated from ambient temperature to 1000 °C at a heating rate of 10 °C/min under a nitrogen atmosphere with a flow rate of 200 mL/min.

2.3.9. Scanning Electron Microscopy-Energy Dispersive X-Ray Spectrometer (SEM-EDS)

The surface morphology and elemental composition of the samples were characterised using scanning electron microscopy coupled with energy dispersive X-ray spectroscopy (SEM–EDX) (JSM-IT300LV, JEOL, Japan). Imaging was carried out in secondary electron mode under vacuum at an accelerating voltage of 5 kV. Micrographs were acquired at magnifications of 500× and 5,000×. Prior to examination, all specimens were coated with a thin layer of platinum to enhance surface conductivity.

3. RESULTS AND DISCUSSION

3.1. Fresh Properties

Figure **4a** presents the flowability of fresh mortar incorporating varying percentages of PODC_Calcined as a partial replacement for FA. A clear decreasing trend in flowability is observed with increasing PODC replacement levels. This reduction in flowability can be attributed to several factors. First, PODC_Calcined has a lower bulk density compared to fly ash (Table **2**). As a result, replacing FA with an equal weight of PODC_Calcined introduces a greater powder volume into the mix thereby increasing the solid content. This reduces the overall water available for lubrication which in turn leads to reduced flowability [28]. Second, FA typically exhibits a smooth, spherical morphology and low surface energy which contribute to a lower liquid limit and facilitate the movement of particles within the mix [29]. In contrast, calcined PODC possesses a rough, irregular surface texture which increases interparticle friction and raises the liquid limit of the system that hindering the flowability of the mix. Additionally, the presence of porous biochar within the PODC_Calcined may contribute to water absorption, reducing the amount of free water in the mix. This characteristic has also been reported in other studies where biochar was found to lower flowability due to its high surface area and water-absorbing capacity [30].

Figure **4b** presents the initial and final setting times of mortars incorporating varying percentages of PODC_Calcined as a partial replacement for FA. The results indicate that the setting times decreased progressively with increasing PODC content. At 20% PODC_Calcined replacement, the initial setting time was reduced by 45.7%, while the final setting time decreased by 15.9%. This reduction can be explained by several mechanisms. Firstly, the biochar present in PODC_Calcined possesses strong water retention properties due to its hydrophilic nature. Biochar can retain approximately 2.5–3.0 times its own weight in water [31]. This behaviour results in a portion of the mixing water being temporarily absorbed and subsequently released during later hydration. However, the immediate effect is a reduction in free water available for alkaline activation which accelerates the reaction and shortens the setting time. This observation is consistent with findings from previous studies which have reported that excessive water retention by biochar may limit the availability of free water in the early stages, leading to faster setting but potentially compromising early-age strength development [32]. Nevertheless, the gradual release of the retained water at later stages sustains the alkaline activation process and leads to additional gel formation, improved matrix densification and enhanced long-term performance. Moreover, the replacement of FA with PODC reduces the setting time partly due to its lower density. The reduced density increases the overall precursor volume which in turn improves the contact area between the solid particles and the alkaline activator thereby facilitating faster dissolution and reaction. In addition, the chemical composition of PODC_Calcined particularly the presence of active calcium, silica and potassium provides further reactive sites that accelerate the alkaline activation process. Calcium promotes the rapid precipitation of binding gels, while silica and potassium enhance aluminosilicate dissolution and gel formation [33, 34]. These combined effects explain the progressive

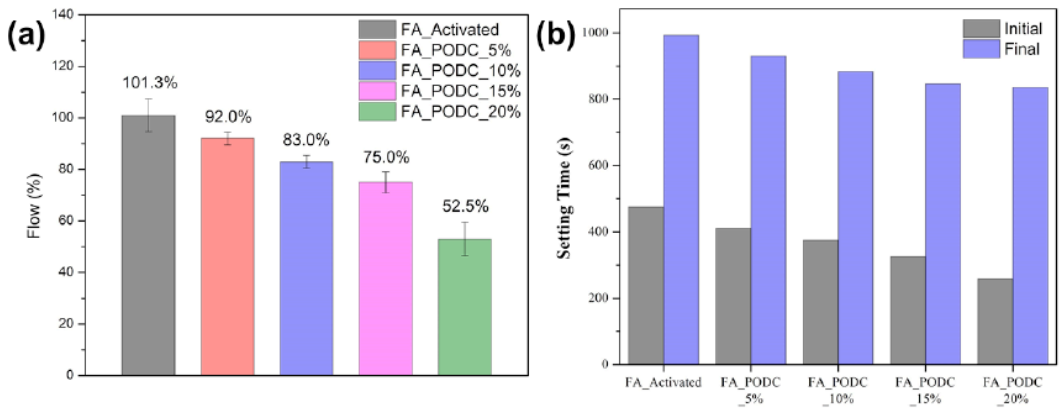

Figure 4: (**a**) Flowability and (**b**) setting time of fresh mortar with PODC_Calcined replacement at different percentages.

reduction in setting time observed with higher levels of PODC replacement.

3.2. Density, adsorption and voids of harden mortars

Figure **5** shows the bulk density of mortar with PODC_Calcined replacement at different percentages. A slight reduction in bulk density is observed with increasing PODC content. This decrease can be attributed to the lower density of PODC_Calcined (2.808g/cm^3) compared to that of fly ash (3.3046g/cm^3). Nevertheless, the reduction is minimal. At 20% PODC replacement, the bulk density at 90 days is only 0.5% lower than the control specimen. Hence, the effect of PODC replacement on the bulk density of mortar can be considered negligible.

Figure **6a** shows the water absorption percentage of mortar with PODC_Calcined incorporated at up to 20% replacement after 28 days of curing. The results indicate that the overall water absorption remains relatively stable at approximately 8% although a gradual increase is observed with higher levels of PODC replacement. This slight increase can be explained by the more porous microstructure of PODC compared to fly ash which introduces additional voids into the mortar matrix as evidenced by the SEM images in Figure **3c**. These voids facilitate the ingress and storage of water leading to a higher measured absorption capacity. Nevertheless, the increase in water absorption is relatively modest compared to other studies where large proportions of biochar replacement resulted in much higher values [35, 36]. This difference may be attributed to the ability of the biochar in PODC to provide nucleation sites for alkaline activation products which subsequently fill part of the pore space and reduce the extent of water uptake [37].

Figure **6b** presents the volume of permeable pore space for mortars incorporating PODC_Calcined as a partial replacement for FA. The increase in pore volume is consistent with the water absorption results shown in Figure **6a** and reflects the influence of PODC's physical and chemical characteristics. Nevertheless, the increase in pore volume is relatively small with only a 0.99% rise at 20% replacement

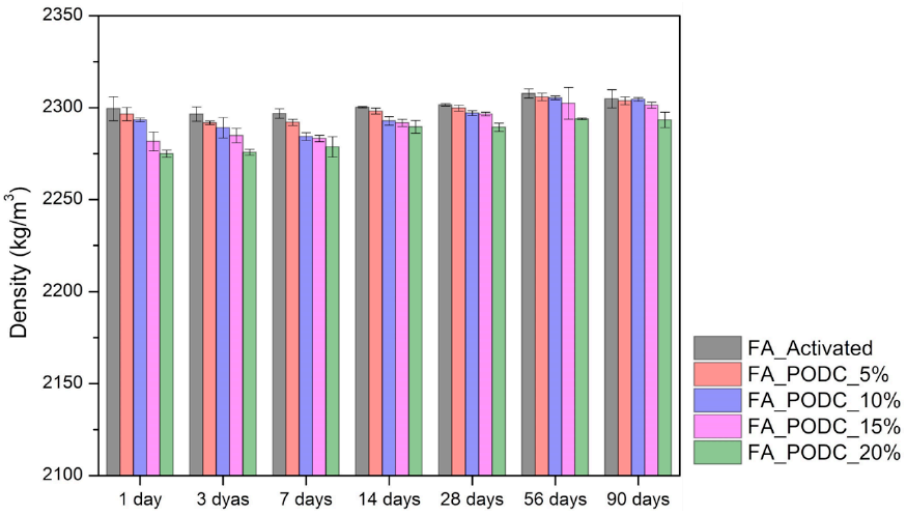

Figure 5: Bulk Density of mortar with PODC_Calcined replacement at different percentages.

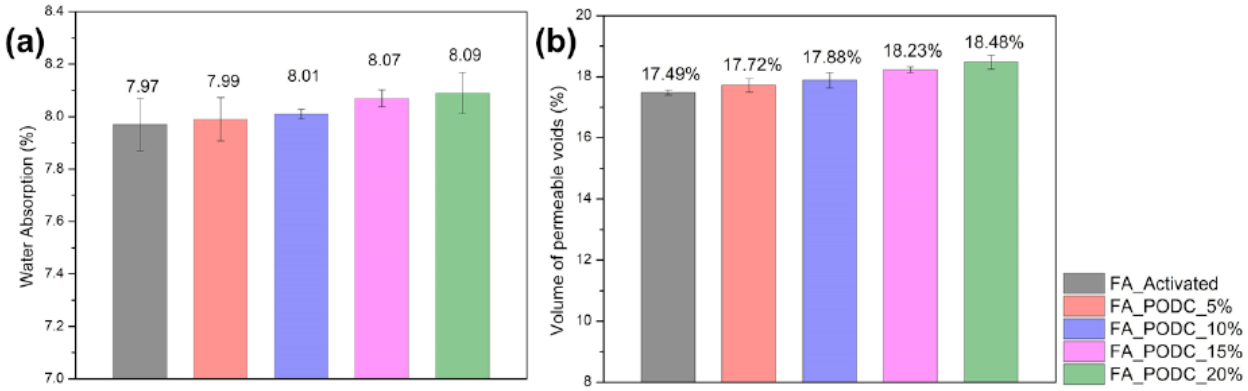

Figure 6: (**a**) Water absorption and (**b**) pores volume of mortar with PODC_Calcined replacement at different percentages at 28 days of curing.

compared to the control specimens. This indicates that while PODC_Calcined incorporation slightly elevates pore connectivity the overall mortar structure remains compact and well refined due to the continued alkaline activation process.

3.3. Compressive Strength

Figure **7** shows the compressive strength of mortars incorporating PODC_Calcined at different replacement levels and curing ages. At the early stage *i.e.*, up to 7 days of curing, mortars with PODC generally exhibited lower compressive strength than the control specimens. Specifically, PODC replacement levels of 5%, 10%, 15%, and 20% resulted in strength reductions of 4.15%, 9.30%, 12.26%, and 10.50%, respectively, relative to the control mix. This behaviour can be attributed to the water retention capacity of PODC_Calcined, which temporarily traps part of the mixing water and reduces its availability for alkaline activation. As a result, fewer binding gels are produced at the early age leading to reduced strength [38, 39]. This water retention effect is consistent with the trends observed in flowability and setting time, as discussed in the previous sections.

Beyond 14 days of curing, the retained water is gradually released, while the biochar in PODC_Calcined provides nucleation sites that facilitate the formation of alkali-activated products. This process enhances gel precipitation, densifies the matrix, and improves strength development [40]. As curing progressed, mortars incorporating PODC_Calcined generally continued to gain strength up to 90 days. However, the FA_PODC_20% mix exhibited a 10.78% reduction in compressive strength compared with the control mix. In the latter case, the excessive presence of biochar hinders the formation of calcium-based binding gels which limits strength development [41]. Besides, the low flowability of fresh FA_PODC_20% (Figure **4a**) and the higher porosity introduced by PODC_Calcined also contribute to its poorer strength performance.

Among the replacement levels, FA_PODC_15% exhibited the best long-term strength performance owing to the availability of reactive K^+, Ca^{2+}, and Si^{2+} in PODC that promote alkali activation. The coexistence of different alkali cation binding gels bridges the gaps

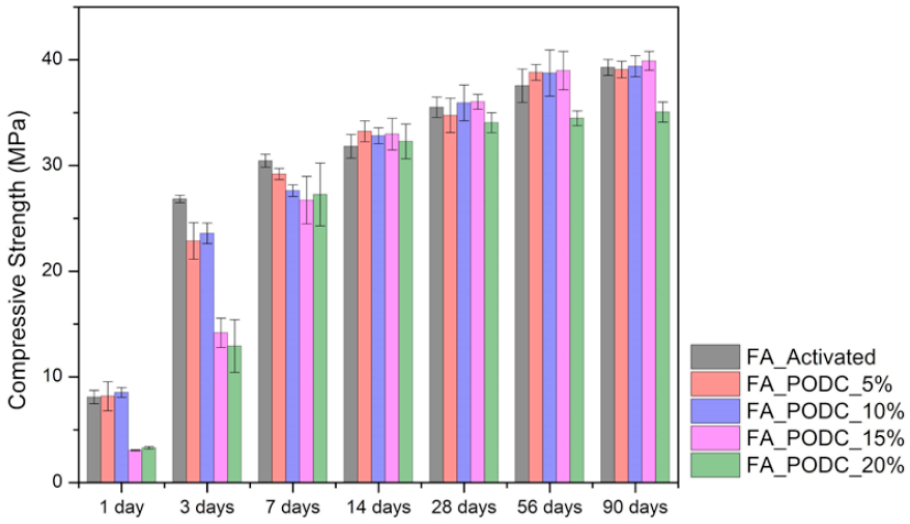

Figure 7: Compressive strength of mortars with PODC_Calcined at different replacement levels and curing ages.

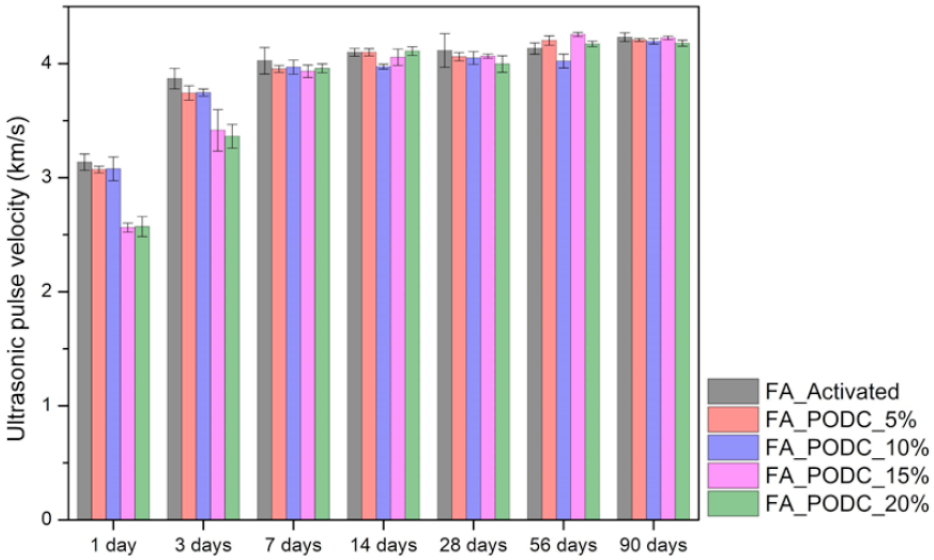

Figure 8: UPV of mortars with PODC_Calcined at different replacement levels and curing ages.

between hydrated phases and unreacted particles, leading to the observed increase in mechanical strength of the binders [42-44]. However, the lower early-age strength of PODC mortars should be taken into consideration for practical applications especially where early load-bearing capacity is critical.

3.4. Ultrasonic Pulse Velocity

Figure **8** shows the UPV of mortars with PODC_Calcined at different replacement levels and curing ages. The UPV trend is closely related to compressive strength with lower values at early ages followed by an increase to a nearly stable level of around 4 km/s. UPV is a well-established non-destructive test for concrete where the measured pulse velocity through the specimen provides an indirect indication of its porosity and strength performance [45]. At 28 days of curing, the UPV results show a clear relationship with the pore volume data presented in Figure **6b**. As the level of PODC replacement increases, a reduction in UPV is observed which corresponds to a rise in the measured pore volume. This confirms that higher amounts of PODC introduce additional porosity resulting in lower pulse velocity. However, UPV continues to increase up to 90 days, indicating that alkaline activation is still progressing beyond 28 days. This improvement is likely due to the gradual release of water retained by the biochar, which sustains the reaction and promotes further matrix densification.

Figure **9** shows the relationship between compressive strength and UPV of mortar with PODC_Calcined at different replacement levels. In view of the inherent heterogeneity of AAM mortar, the relationship was established by combining all mortar data obtained between 1 and 90 days of curing. The relationship follows an exponential trend, with an R^2 value greater than 0.92. This indicates that at least 92% of the variation in the values of compressive strength is accounted for by exponential relationship with UPV. Furthermore, previous studies have also reported similar exponential relationships between compressive strength and UPV in different types of concrete [46-48].

3.5. Flexural Strength

Figure **10** shows the flexural strength of 28 days cured mortar with PODC_Calcined at different replacement levels. Compared with the reference specimen (FA_Activated), the 10% and 15% PODC_Calcined mixes exhibited notable increases in flexural strength of 12.8% and 17.9%, respectively. In contrast, the 5% and 20% replacement levels resulted in reductions of 8.7% and 14.7%, respectively.

The improvement observed at 10% and 15% replacement can be attributed to the porous structures of biochar, which facilitates penetration of the alkali-activated matrix and creates mechanical interlocking during curing [49]. Moreover, the fine particle size of biochar provides a micro-filler effect, leading to improved matrix densification and more efficient stress transfer [50]. Conversely, the strength reduction at 20% replacement is likely due to the excessive amount of biochar, which promotes the formation of additional air voids and weak zones during curing. The presence of such voids decreases the energy needed for cracks to propagate, thereby restricting the mortar's ability to sustain flexural loads [51]. The reduction at 5% replacement may be related to the corresponding drop in compressive strength, as

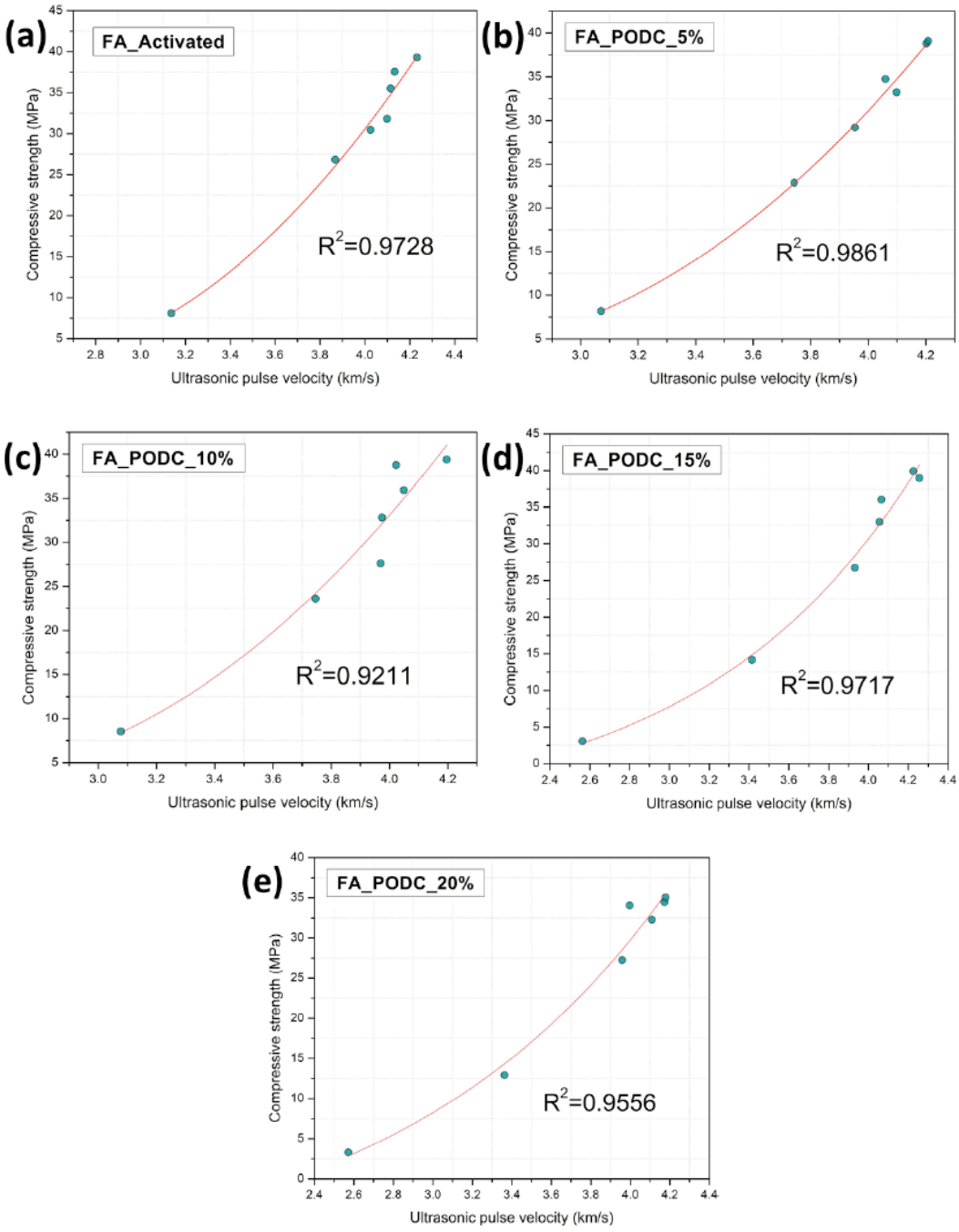

Figure 9: Relationship of compressive strength and UPV of mortar with PODC_Calcined at different replacement levels.

flexural and compressive strength are closely correlated, as shown in Figure **7** [50].

Figure **11** illustrates the relationship between flexural strength and compressive strength of mortars incorporating PODC_Calcined at different replacement levels. The overall trend follows the empirical power law function proposed by Neville [52] (Equation 1), where f_r denotes flexural strength, f_c denotes compressive strength and k and α are empirical constants. Although these constants vary depending on the type of concrete or mortar, OPC mortar values are used here as a reference for comparison, with k typically ranging from 0.5 to 0.7 and α from 0.5 to 0.75 [52-54]. Accordingly, the upper limit for OPC mortar is plotted as a red line and the lower limit as a green line in Figure **6**.**10**. The AAMs mortars incorporating PODC at different replacement levels exhibit a non-linear quadratic relationship between flexural and compressive strength, which diverges from the classical empirical power law observed in OPC mortars (Equation 1). This deviation may be attributed to the distinct gel chemistry of alkali-activated binders, where multiple reaction products such as (N,K)-A-S-H, N-A-S-H, C-A-S-H, and C-S-H coexist, rather than the dominant C–S–H found in OPC. Furthermore, the incorporation of PODC introduces microstructural heterogeneity, including additional porosity and

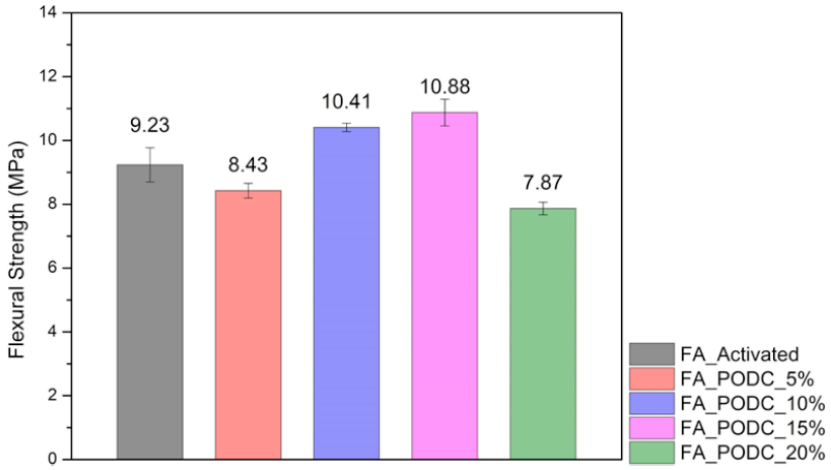

Figure 10: Flexural strength of mortar with PODC_Calcined at different replacement levels.

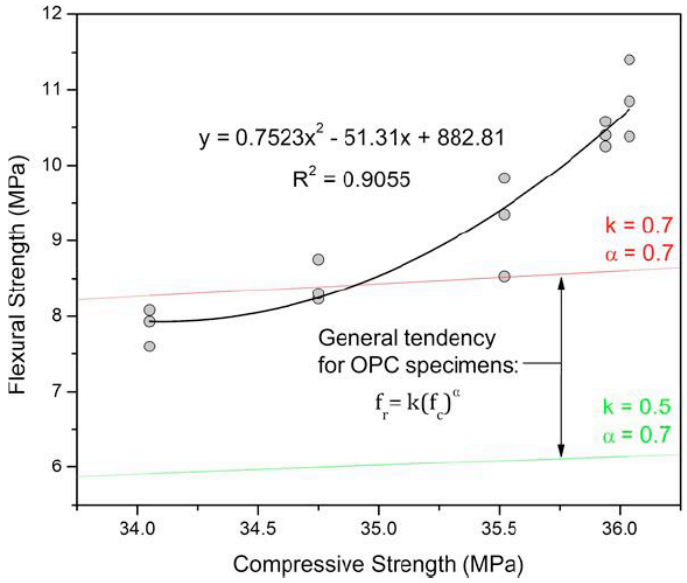

Figure 11: Relationship of flexural strength and compressive strength of mortar with PODC_400 °C at different replacement levels.

irregular particle interfaces, which affects flexural performance more sensitively than compressive strength. The presence of biochar at lower replacement levels provides micro-filler and mechanical interlocking effects that enhance flexural strength, whereas excessive additions promote void formation and weak zones that accelerate crack propagation. Together, these factors explain the departure from the conventional power-law trend and the emergence of a quadratic correlation between flexural and compressive strength in FA–PODC AAMs mortars.

$$f_r = k(f_c)^{\alpha} \quad \text{(Equation 1)}$$

3.6. Splitting Tensile Strength

Figure **12** shows the splitting tensile strength of 28-day cured mortars with PODC_Calcined at different replacement levels. Compared with the reference specimen (FA_Activated), the 10% and 15% PODC_Calcined mixes exhibited increases of 3.31% and 8.28%, respectively. In contrast, the 5% and 20% replacement levels showed reductions of 2.9% and 12.42%, respectively. The splitting tensile strength shows a similar trend to the flexural strength, but the improvement is less significant. Similar observations have been reported by other researchers, who noted that biochar particles tend to promote the formation of additional air voids, thereby increasing the heterogeneity of the tensile plane [55, 56]. The increase in splitting tensile strength for FA_PODC_10% and FA_PODC_15% can be attributed to the optimum dosage of biochar, which enhances crack bridging and provides additional pathways for stress redistribution, thereby improving resistance to brittle failure [56]. In contrast, the strength reduction observed at 20% PODC_Calcined replacement is due to the excessive amount of biochar,

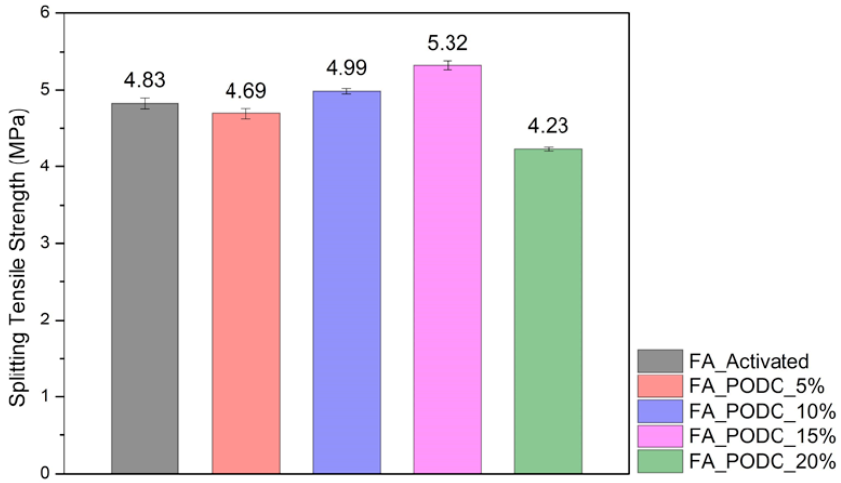

Figure 12: Splitting tensile strength of mortar with PODC_Calcined at different replacement levels.

which generates voids and weakens the Interfacial Transition Zone (ITZ) [38].

Figure **13** illustrates the relationship between splitting tensile strength and compressive strength of mortars incorporating PODC_Calcined at different replacement levels. The correlation is non-linear, indicating that although splitting tensile strength increases with compressive strength, the rate of increase is comparatively lower. Generally, this trend can be described by the empirical power law function proposed by various researchers (Equation 2), where f_{ct} represents splitting tensile strength, f_c represents compressive strength, and k and α are empirical constants [52, 57]. For reference, the upper limit shown as a red line corresponds to the research of ultra-high-performance concrete from Arıoglu *et al.* [58], while the lower limit shown as a green line follows ACI-318 [59]. The AAMs mortars incorporating PODC at different replacement levels show a non-linear quadratic relationship between splitting tensile and compressive strength, similar to relationship between flexural strength and compressive strength from the previous section. This behaviour is linked to the complex gel chemistry of alkali-activated binders, where multiple reaction products coexist, and to the microstructural effects of PODC. At moderate replacement levels, biochar contributes to micro-filler and crack-bridging effects that enhance tensile performance, whereas excessive additions increase porosity and weak zones, reducing strength. These combined factors account for the deviation from the conventional OPC trend.

$$f_{ct} = k(f_c)^{\alpha} \quad \text{(Equation 2)}$$

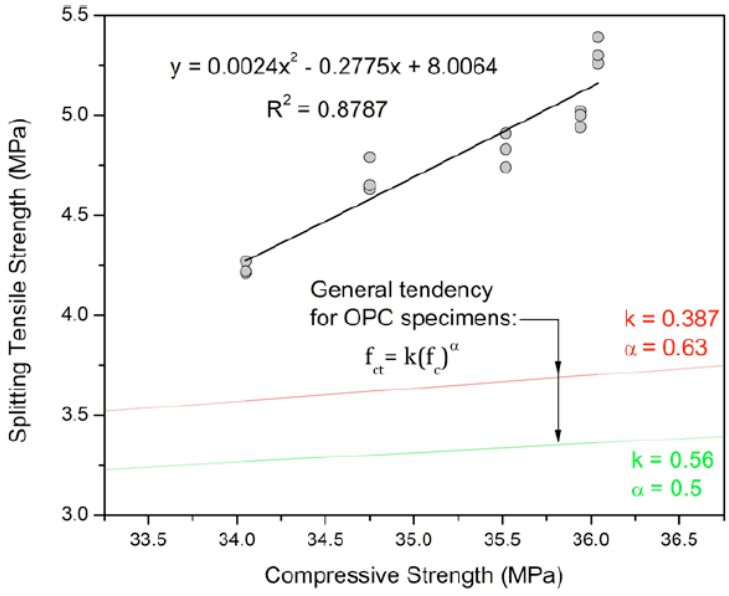

Figure 13: Relationship of splitting tensile strength and compressive strength of mortar with PODC_Calcined at different replacement levels.

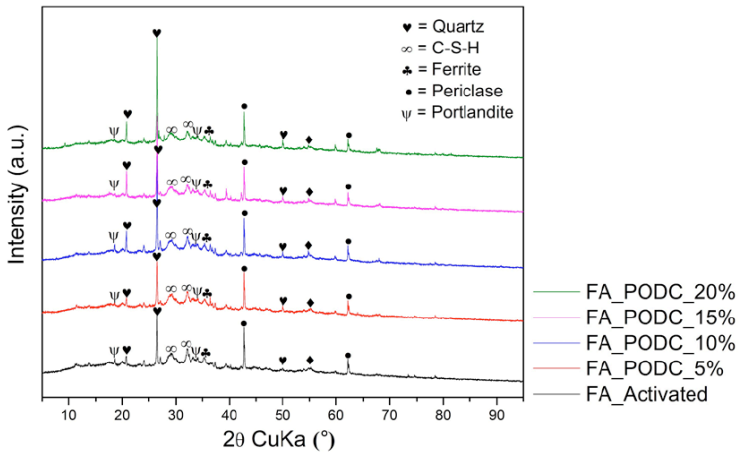

Figure 14: XRD pattern of FA-PODC AAMs incorporating different PODC replacement percentages at 28 days.

3.7. Crystallinity

Figure **14** presents the XRD patterns of FA-PODC AAMs incorporating different PODC replacement levels at 28 days. In each plot, the reference XRD profile of the raw materials was superimposed onto that of the AAMs to highlight which crystalline phases were consumed during the alkaline activation process. For comparison, the control specimen (FA_Activated) is shown beneath the corresponding AAMs patterns.

The results indicate that the inclusion of PODC_Calcined does not produce significant differences in crystalline phases compared with the FA_Activated control, even at 20% replacement. This outcome can be attributed to the fact that most phases in PODC_400 °C are readily dissolved and consumed during alkaline activation, contributing instead to the broad amorphous hump between 18° and 35° 2θ [60]. In addition to these phase transformations, the improved performance of FA-PODC mortars can also be linked to the presence of biochar, which mechanically enhances the ITZ by acting as a reinforcing centroid. Therefore, the role of PODC in AAM is reflected less in the crystalline fingerprint of the hardened matrix and more in the amorphous phase development and microstructural refinement.

3.8. Thermal Behaviour

Figure **15** shows the TG and DTA of FA-PODC AAMs incorporating different PODC replacement percentages at 28 days. According to Figure **15a**, FA_PODC_20% exhibited the greatest weight loss due to thermal decomposition up to 1000 °C, while FA_Activated showed the lowest. This behaviour can be explained by the excess biochar present in the system, which increases porosity and captures more water, consistent with the water absorption results shown in Figure **6a**. By contrast, the FA_PODC_10% and FA_PODC_15% mixes displayed weight loss behaviour comparable to that of FA_Activated, indicating good thermal stability despite the presence of biochar. Among these, FA_PODC_15% exhibited the most favourable balance between thermal stability and mechanical performance, reflecting an optimal biochar content that contributes to matrix densification rather than porosity generation. This suggests that, at optimum replacement levels, biochar no longer exists as free pores but instead acts as a structural centroid around which the AAMs binding gels densify, resulting in a stronger matrix.

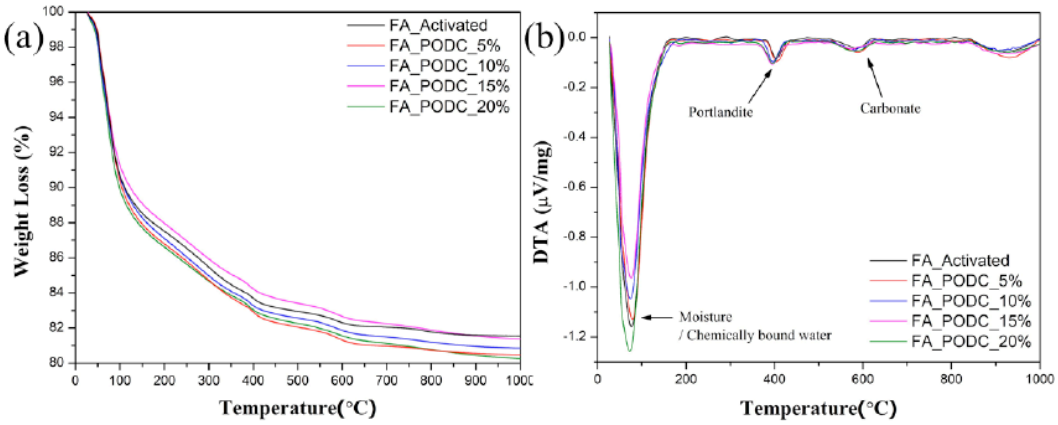

Figure 15: TG-DTA of FA-PODC AAM incorporating different PODC replacement percentages at 28 days.

As illustrated in Figure **15b**, three main decomposition peaks can be identified. The first, around 200 °C, corresponds to the release of physically adsorbed moisture and chemically bound water from the AAMs binding gels [61]. The second, near 400 °C, is associated with the dehydroxylation of portlandite ($Ca(OH)_2$) [62]. Given that Class C fly ash, which is rich in reactive calcium, was used as the primary precursor, excess Ca^{2+} may hydrate during mixing and persist as crystalline portlandite within the matrix [63]. The third peak, around 600 °C, is attributed to the decomposition of carbonate phases [64]. These carbonates may originate from carbonated free Ca^{2+} or from calcite formed through the decomposition of whewellite present in raw PODC. Accordingly, FA_Activated exhibited the lowest carbonate loss among all mixes, as it does not contain whewellite.

3.9. Morphology and Elemental Features

Figure **16** displays the SEM images and EDX elemental mapping of the control FA_Activated samples cured for 28 days, captured at ×5000 magnification. The EDX analysis highlights the distribution of key elements, namely Ca, Na, Si, K, Al, and O, which are critical indicators of the reaction products formed during alkali activation. The microstructure of FA_Activated reveals a relatively homogeneous binding matrix composed of a mixture of C–S–H, C–A–S–H, and N–A–S–H type gels. Previous studies have also shown that in high-calcium AAMs systems, C–S–H gel can coexist alongside alkali-activated gels [65, 66]. These gels coexist in close association, reflecting the high-calcium nature of the Class C FA and its ability to generate both calcium-rich and aluminosilicate-rich phases.

Figure **17a** shows the SEM–EDX mapping of FA_PODC_5% cured for 28 days. The microstructure appears relatively dense and homogeneous, consisting of both calcium-based gels (C–S–H and C–A–S–H) and alkali metal-based gels ((N,K)–A–S–H). However, the potassium signal in the EDX mapping is noticeably weaker compared to specimens with higher PODC_Calcined replacement. This can be explained by the fact that PODC is the main source of potassium in the system, and the lower replacement level results in reduced potassium availability, which is directly reflected in the EDX indicator.

Figure **17b**, **c**, and **d** correspond to higher PODC_Calcined replacement levels, where the elemental distribution becomes more clearly differentiated between calcium-rich and alkali metal-rich regions. The calcium-based gels generally appear as cloudy, diffuse phases, while the alkali metal-based gels are observed as larger, blocky domains. This distinction highlights the coexistence and interaction of different binding phases in FA–PODC AAMs, with their relative proportions influenced by the level of PODC replacement. The increasing prominence of potassium-rich phases at higher replacement levels also confirms the contribution of PODC in modifying the gel chemistry and potentially enhancing long-term performance. Identifying the presence of biochar within the matrix was challenging, as it is likely dispersed at the nanoscale and embedded within the AAMs gel. This supports the earlier hypothesis that biochar serves as a centroid around which the alkali-activated gel network develops, rather than existing as distinct or isolated phases detectable by SEM–EDX.

3.9. Sustainability Implications

The development of FA–PODC one-part AAMs mortars offers both sustainability and performance advantages when benchmarked against conventional OPC binders and recently reported waste-based AAMs systems. Unlike OPC production, which relies on energy-intensive clinkerisation at temperatures exceeding 1350 °C [67], the present system utilises industrial fly ash and palm oil decanter cake (PODC), with the latter subjected to low-temperature calcination

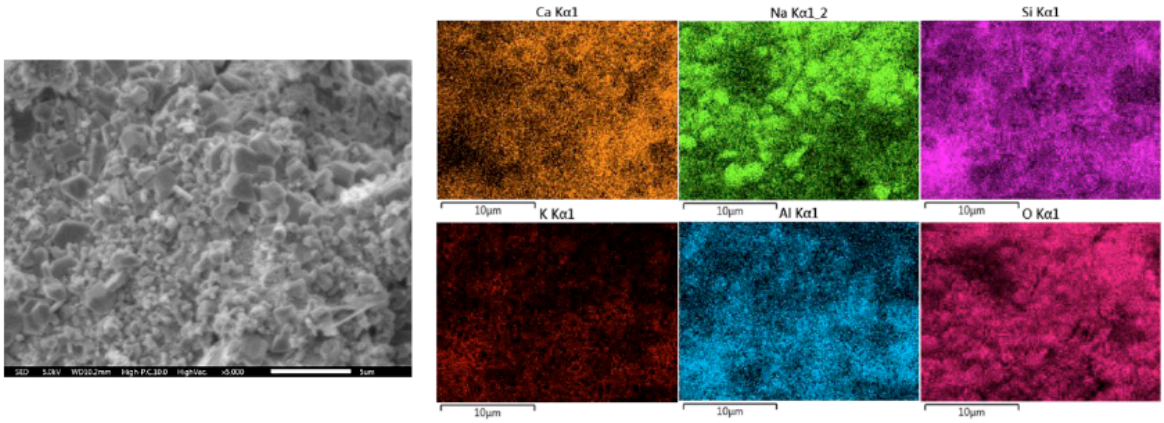

Figure 16: SEM-EDX of FA_Activated sample.

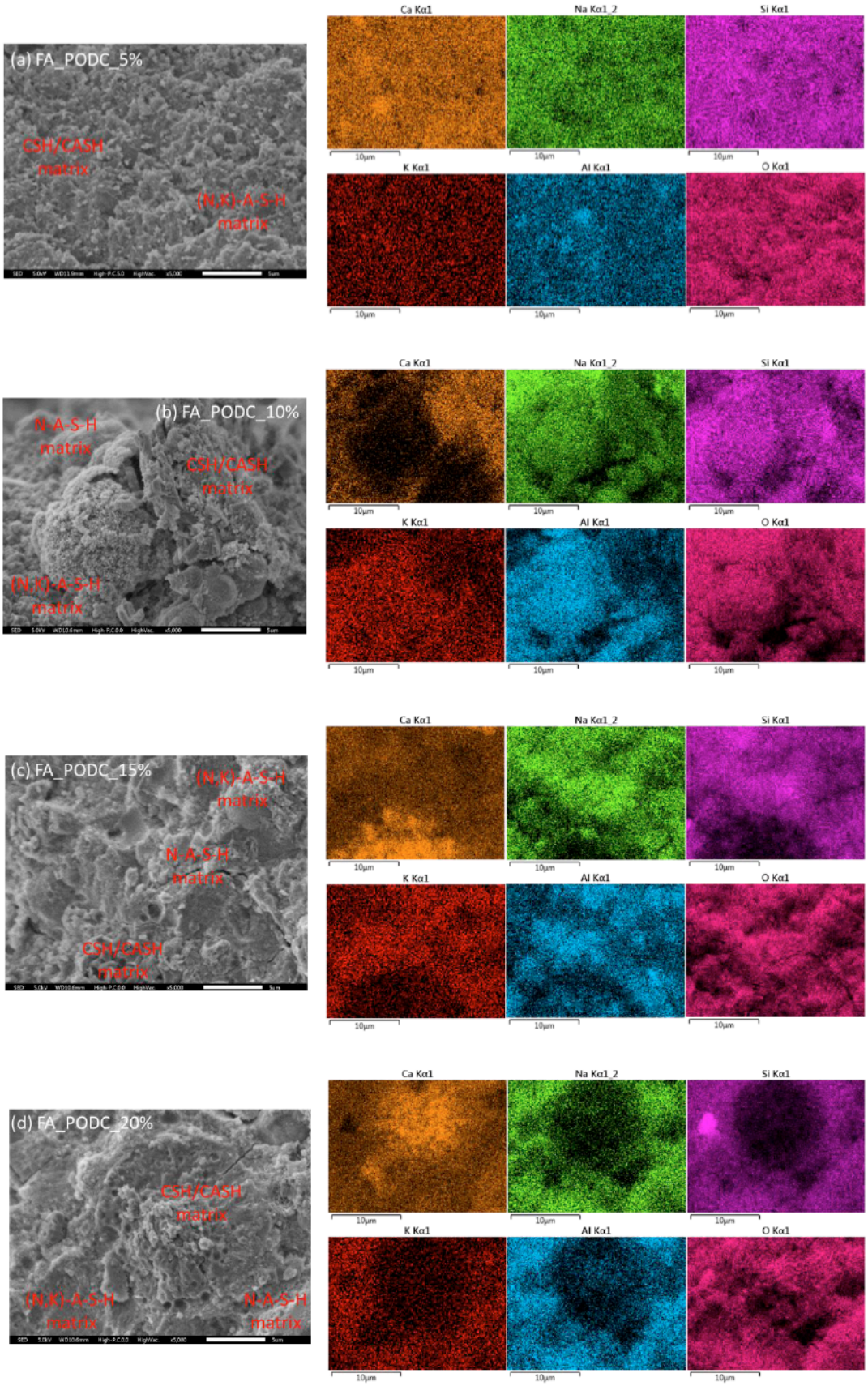

Figure 17: SEM-EDX of FA-PODC AAMs incorporated with different replacement percentages.

at 400 °C. This substantially reduces the embodied energy associated with binder production while promoting the valorisation of agricultural waste streams that are otherwise underutilised or landfilled.

Beyond energy considerations, the use of PODC contributes to improved resource efficiency and waste management within the palm oil industry, where PODC is often stockpiled or disposed of with limited value

recovery [68]. Converting PODC into a functional binder component supports circular economy principles by transforming an agricultural residue into a value-added construction material. Additionally, the carbon-rich nature of PODC-derived biochar introduces the potential for partial carbon retention within the hardened matrix, which may contribute to long-term carbon storage, although this aspect requires further dedicated investigation.

Recent studies on FA–based AAMs materials have shown that the incorporation of alternative waste or biomass-derived additives, such as rice husk ash [69], palm oil fuel ash [70], and wood ash [71], can provide beneficial effects when appropriately optimised. These materials have been reported to enhance microstructural densification, modify gel chemistry, and improve mechanical performance by contributing additional reactive species or refining the interfacial transition zone of the binder matrix [72]. In this context, the incorporation of calcined PODC in the present study exhibits comparable beneficial behaviour. At an optimum replacement level of 15%, PODC addition results in enhanced 28-day compressive strength, a dense and well-integrated microstructure, and stable thermal behaviour. These observations are consistent with trends reported for other waste-modified FA-based AAM systems [73], demonstrating that agricultural waste-derived materials, when properly processed and dosed, can function effectively as performance-enhancing components rather than inert fillers. Accordingly, PODC may be considered a locally relevant alternative to other biomass-derived additives reported in the literature, offering similar functional benefits while supporting waste valorisation and practical one-part binder formulation.

4. CONCLUSION

This study evaluated the effects of partially replacing FA with calcined PODC at replacement levels of 5–20% on the fresh, mechanical and microstructural performance of one-part AAMs mortar systems. The incorporation of PODC was found to influence fresh properties, with increasing replacement levels leading to reduced flowability and shortened setting times. These effects are attributed to the lower density, irregular particle morphology and water-retention behaviour associated with biochar present in PODC. Despite these changes, bulk density, water absorption and apparent porosity were only marginally affected, indicating that the overall compactness of the hardened matrix was largely maintained.

Mechanical performance was strongly dependent on the replacement level. Mortars containing 10% and 15% PODC_Calcined exhibited superior strength development compared with the control mixture. The 15% replacement achieved the highest long-term compressive strength, benefitting from additional reactive calcium, potassium and silica contributed by PODC. Meanwhile, the 10% replacement demonstrated a more balanced performance, characterised by improved workability, stable early-age strength, and enhanced flexural and splitting tensile strengths. In contrast, a 20% replacement level resulted in noticeable strength degradation, which is associated with excessive porosity and the formation of a weaker interfacial transition zone.

Microstructural and thermal analyses corroborated the mechanical findings. XRD results indicated substantial consumption of PODC phases during activation, contributing to the formation of amorphous reaction products. TG–DTA profiles revealed typical decomposition features associated with bound water, portlandite and carbonates, consistent with the high-calcium characteristics of Class C FA systems. SEM–EDS observations confirmed the presence of well-developed binding gels, including C–S–H, C–A–S–H and alkali-substituted (N,K)–A–S–H phases, and highlighted the contribution of potassium-rich components introduced by PODC. The residual biochar acted as a preferential site for gel nucleation, enhancing interfacial bonding and overall matrix cohesion.

Overall, the results demonstrate that PODC_Calcined can be effectively utilised as a partial fly ash replacement in one-part alkali-activated mortars. An optimal replacement range of 10–15% is identified, with 15% maximising strength performance and 10% providing a more practical balance between workability, early-age behaviour and long-term mechanical properties. These findings highlight the potential of calcined PODC as a sustainable supplementary precursor for the development of high-performance one-part alkali-activated systems. Further research is recommended to investigate the durability, high-temperature resistance and interfacial bonding behaviour of PODC-modified one-part AAM systems under aggressive service conditions.

ACKNOWLEDGMENT

This research was supported by Universiti Teknologi Malaysia (UTM) under the UTM Fundamental Research Grant (Q.J130000.3822.24H26 and Q.J130000.3822.24H40).

CONFLICTS OF INTEREST

The authors declare that they have no known competing financial interests or personal relationships

that could have appeared to influence the work reported in this paper.

REFERENCES

[1] M. Hanifa, R. Agarwal, U. Sharma, P.C. Thapliyal, L.P. Singh, A review on CO2 capture and sequestration in the construction industry: Emerging approaches and commercialised technologies, Journal of CO2 Utilization 67 (2023) 102292. https://doi.org/10.1016/j.jcou.2022.102292

[2] A.A. Alrawashdeh, M. Zamorano, M. Alshaaer, M. Martín-Morales, Promoting the use of geopolymer and alkali-activated materials through the identification of critical factors and strategies, Journal of Building Engineering 98 (2024) 111078. https://doi.org/10.1016/j.jobe.2024.111078

[3] Y.T. Chan, N.H. Abdul Shukor Lim, S.A. Abd Latif, S. Ishak, P.S. Lee, S.Q. Tan, A. Azhar, J.J. Moy, H.Y. Kek, Scientometric Review of One-Part Geopolymer Composites, in: M. Khandelwal, E.T. Mohamad, R. Bhatawdekar, D.J. Armaghani, P. Asteris, P.N. Shek, C.K. Ma (Eds.) Proceedings of the Innovative and Sustainable Infrastructure International Convention, Springer Nature Singapore, Singapore, 2025, pp. 407-416. https://doi.org/10.1007/978-981-96-3804-8_36

[4] P. Nuaklong, A. Wongsa, V. Sata, K. Boonserm, J. Sanjayan, P. Chindaprasirt, Properties of high-calcium and low-calcium fly ash combination geopolymer mortar containing recycled aggregate, Heliyon 5(9) (2019) e02513. https://doi.org/10.1016/j.heliyon.2019.e02513

[5] M.J. McCarthy, H.I. Yakub, L.J. Csetenyi, Impact of fly ash production and sourcing changes on chemical and physical aspects of concrete durability, Construction and Building Materials 342 (2022) 127313. https://doi.org/10.1016/j.conbuildmat.2022.127313

[6] M.N.A. Razak, M.F. Ibrahim, P.L. Yee, M.A. Hassan, S. Abd-Aziz, Utilization of oil palm decanter cake for cellulase and polyoses production, Biotechnology and Bioprocess Engineering 17(3) (2012) 547-555. https://doi.org/10.1007/s12257-011-0590-9

[7] P. Wu, K. Dai, Y. Shi, H. Rong, X. Zhang, Effect of biomass ash on hydration, properties and microstructure of ultra-high performance concrete, Journal of Building Engineering 104 (2025) 112276. https://doi.org/10.1016/j.jobe.2025.112276

[8] N.A. Rahim, N.Y. Harun, A.A.H. Saeed, M.R. Bilad, Green route synthesis of amorphous silica from oil palm decanter cake: From literature review to experiments, Indonesian Journal of Science and Technology 8(2) (2023) 141-156. https://doi.org/10.17509/ijost.v8i2.53724

[9] Y.T. Chan, N.H.A.S. Lim, S. Ishak, S.Q. Tan, S.A.A. Latif, S.P. Ngian, J.J. Moy, H.Y. Kek, A Review of Trends and Technologies Advancing Concrete with Biochar, in: K.-C. Tsai, M. Shahin, S.A. Kristiawan, A.R.M. Sam, P.D. Hai (Eds.) Proceedings of the 6th International Conference on Rehabilitation and Maintenance in Civil Engineering—Volume 1, Springer Nature Singapore, Singapore, 2025, pp. 191-199. https://doi.org/10.1007/978-981-96-2143-9_21

[10] G. Murali, L.S. Wong, A comprehensive review of biochar-modified concrete: Mechanical performance and microstructural insights, Construction and Building Materials 425 (2024) 135986. https://doi.org/10.1016/j.conbuildmat.2024.135986

[11] H. Egodagamage, H.D. Yapa, H.A.D. Samith Buddika, S. Navaratnam, K. Nguyen, Effective use of biochar as an additive for alkali-activated slag mortar production, Construction and Building Materials 370 (2023) 130487. https://doi.org/10.1016/j.conbuildmat.2023.130487

[12] ASTM C618, Standard Specification for Coal Fly Ash and Raw or Calcined Natural Pozzolan for Use in Concrete, ASTM International, West Conshohocken, 2022, p. 5.

[13] D. Chen, D. Liu, H. Zhang, Y. Chen, Q. Li, Bamboo pyrolysis using TG–FTIR and a lab-scale reactor: Analysis of pyrolysis behavior, product properties, and carbon and energy yields, Fuel 148 (2015) 79-86. https://doi.org/10.1016/j.fuel.2015.01.092

[14] Z. Zhang, H. Wang, J.L. Provis, Quantitative study of the reactivity of fly ash in geopolymerization by FTIR, Journal of Sustainable Cement-Based Materials 1(4) (2012) 154-166. https://doi.org/10.1080/21650373.2012.752620

[15] N. Kanjana, W. Maiaugree, P. Laokul, I. Chaiya, T. Lunnoo, P. Wongjom, Y. Infahsaeng, B. Thongdang, V. Amornkitbamrung, Fly ash boosted electrocatalytic properties of PEDOT:PSS counter electrodes for the triiodide reduction in dye-sensitized solar cells, Scientific Reports 13(1) (2023) 6012. https://doi.org/10.1038/s41598-023-33020-6

[16] ASTM C430, Standard Test Method for Fineness of Hydraulic Cement by the 45-µm (No. 325) Sieve, ASTM International, West Conshohocken, 2017, p. 3.

[17] C. Chandara, E. Sakai, K.A.M. Azizli, Z.A. Ahmad, S.F.S. Hashim, The effect of unburned carbon in palm oil fuel ash on fluidity of cement pastes containing superplasticizer, Construction and Building Materials 24(9) (2010) 1590-1593. https://doi.org/10.1016/j.conbuildmat.2010.02.036

[18] M.S. Reza, S. Afroze, M.S.A. Bakar, R. Saidur, N. Aslfattahi, J. Taweekun, A.K. Azad, Biochar characterization of invasive Pennisetum purpureum grass: effect of pyrolysis temperature, Biochar 2(2) (2020) 239-251. https://doi.org/10.1007/s42773-020-00048-0

[19] A.A. Maamoun, R.M. Abouomar, T.M. El-Basheer, M.A. Azab, *E.G.* Zaki, S.M. Elsaeed, A. Elkhateeb, Improving the acoustic performance of flexible polyurethane foam using biochar modified by (3-aminopropyl)trimethoxysilane coupling agent, Scientific Reports 14(1) (2024) 18382. https://doi.org/10.1038/s41598-024-68039-w

[20] R. Snellings, J. Chwast, Ö. Cizer, N. De Belie, Y. Dhandapani, P. Durdzinski, J. Elsen, J. Haufe, D. Hooton, C. Patapy, M. Santhanam, K. Scrivener, D. Snoeck, L. Steger, S. Tongbo, A. Vollpracht, F. Winnefeld, B. Lothenbach, Report of TC 238-SCM: hydration stoppage methods for phase assemblage studies of blended cements—results of a round robin test, Materials and Structures 51(4) (2018) 111. https://doi.org/10.1617/s11527-018-1237-5

[21] ASTM C191, Standard Test Methods for Time of Setting of Hydraulic Cement by Vicat Needle, ASTM International, West Conshohocken, 2021, p. 8.

[22] ASTM C1437, Standard Test Method for Flow of Hydraulic Cement Mortar, ASTM International, West Conshohocken, 2020, p. 2.

[23] ASTM C642, Standard Test Method for Density, Absorption, and Voids in Hardened Concrete, ASTM International, West Conshohocken, 2021, p. 3.

[24] ASTM C597, Standard Test Method for Ultrasonic Pulse Velocity Through Concrete, ASTM International, West Conshohocken, 2022, p. 4.

[25] ASTM C109, Standard Test Method for Compressive Strength of Hydraulic Cement Mortars (Using 2-in. or [50-mm] Cube Specimens), ASTM International, West Conshohocken, 2022, p. 11.

[26] ASTM C348, Standard Test Method for Flexural Strength of Hydraulic-Cement Mortars, ASTM International, West Conshohocken, 2021, p. 6.

[27] ASTM C496, Standard Test Method for Splitting Tensile Strength of Cylindrical Concrete Specimens, ASTM International, West Conshohocken, 2017, p. 4.

[28] N. Roussel, T.L.H. Nguyen, O. Yazoghli, P. Coussot, Passing ability of fresh concrete: A probabilistic approach, Cement and Concrete Research 39(3) (2009) 227-232. https://doi.org/10.1016/j.cemconres.2008.11.009

[29] M. Zhao, X. Zhang, Y. Zhang, Effect of free water on the flowability of cement paste with chemical or mineral admixtures, Construction and Building Materials 111 (2016) 571-579. https://doi.org/10.1016/j.conbuildmat.2016.02.057

[30] S. Gupta, A. Kashani, Utilization of biochar from unwashed peanut shell in cementitious building materials – Effect on early age properties and environmental benefits, Fuel Processing Technology 218 (2021) 106841. https://doi.org/10.1016/j.fuproc.2021.106841

[31] X. Yang, X.-Y. Wang, Hydration-strength-durability-workability of biochar-cement binary blends, Journal of Building Engineering 42 (2021) 103064. https://doi.org/10.1016/j.jobe.2021.103064

[32] K. Tan, X. Pang, Y. Qin, J. Wang, Properties of cement mortar containing pulverized biochar pyrolyzed at different temperatures, Construction and Building Materials 263 (2020) 120616. https://doi.org/10.1016/j.conbuildmat.2020.120616

[33] Y. Li, T. Song, H. Lin, J. Shen, Ambient-temperature properties and mechanistic insights of calcium oxalate-modified low-calcium fly ash geopolymer: Eliminating the need for high-temperature activation, Case Studies in Construction Materials 22 (2025) e04477. https://doi.org/10.1016/j.cscm.2025.e04477

[34] P. Scanferla, A. Gharzouni, N. Texier-Mandoki, X. Bourbon, S. Rossignol, Effects of potassium-silicate, sands and carbonates concentrations on metakaolin-based geopolymers for high-temperature applications, Open Ceramics 10 (2022) 100257. https://doi.org/10.1016/j.oceram.2022.100257

[35] S. Kushwah, S. Singh, R. Agarwal, N.S. Nighot, R. Kumar, H. Athar, S. Naik B, Mixture of biochar as a green additive in cement-based materials for carbon dioxide sequestration, Journal of Materials Science: Materials in Engineering 19(1) (2024) 27. https://doi.org/10.1186/s40712-024-00170-y

[36] S. Gupta, A. Kashani, A.H. Mahmood, T. Han, Carbon sequestration in cementitious composites using biochar and fly ash – Effect on mechanical and durability properties, Construction and Building Materials 291 (2021) 123363. https://doi.org/10.1016/j.conbuildmat.2021.123363

[37] Y. Zhou, S. Wang, L. Chen, Progress and prospects of biochar as concrete filler: A review, Alexandria Engineering Journal 128 (2025) 306-323. https://doi.org/10.1016/j.aej.2025.05.077

[38] R. Patel, J. Stobbs, B. Acharya, Study of biochar in cementitious materials for developing green concrete composites, Scientific Reports 15(1) (2025) 22192. https://doi.org/10.1038/s41598-025-07210-3

[39] F. Wu, Q. Zhang, S. Dong, Y. Cai, S. Yang, F. Xu, P. Luo, J. Jiang, Biochar modification enhances mechanical and durability properties of cement-based materials, Scientific Reports 15(1) (2025) 22174. https://doi.org/10.1038/s41598-025-06968-w

[40] D. Wang, A. Jantwal, E. Kaynak, G. Sas, O. Das, Promoting internal curing in concrete by replacing sand with sustainable biochar, Case Studies in Construction Materials 22 (2025) e04542. https://doi.org/10.1016/j.cscm.2025.e04542

[41] A. Sirico, P. Bernardi, C. Sciancalepore, F. Vecchi, A. Malcevschi, B. Belletti, D. Milanese, Biochar from wood waste as additive for structural concrete, Construction and Building Materials 303 (2021) 124500. https://doi.org/10.1016/j.conbuildmat.2021.124500

[42] C.K. Yip, G.C. Lukey, J.S.J. van Deventer, The coexistence of geopolymeric gel and calcium silicate hydrate at the early stage of alkaline activation, Cement and Concrete Research 35(9) (2005) 1688-1697. https://doi.org/10.1016/j.cemconres.2004.10.042

[43] M.A. Gómez-Casero, L. Pérez-Villarejo, P.J. Sánchez-Soto, D. Eliche-Quesada, Comparative study of alkali activated cements based on metallurgical slags, in terms of technological properties developed, Sustainable Chemistry and Pharmacy 29 (2022) 100746. https://doi.org/10.1016/j.scp.2022.100746

[44] A. Hosan, S. Haque, F. Shaikh, Compressive behaviour of sodium and potassium activators synthetized fly ash geopolymer at elevated temperatures: A comparative study, Journal of Building Engineering 8 (2016) 123-130. https://doi.org/10.1016/j.jobe.2016.10.005

[45] M.A.d.N. Moura, A.L. Moreno, G.C.d.S. Ferreira, Ultrasonic testing on evaluation of concrete residual compressive strength: A review, Construction and Building Materials 373 (2023) 130887. https://doi.org/10.1016/j.conbuildmat.2023.130887

[46] A. Srivastava, S.K. Singh, C.S. Sharma, Correlation Between Ultrasonic Pulse Velocity (UPV) and Compressive Strength of Coal Bottom Ash Mortar, Journal of The Institution of Engineers (India): Series A 102(2) (2021) 421-433. https://doi.org/10.1007/s40030-021-00521-4

[47] S.A. Omer, R. Demirboga, W.H. Khushefati, Relationship between compressive strength and UPV of GGBFS based geopolymer mortars exposed to elevated temperatures, Construction and Building Materials 94 (2015) 189-195. https://doi.org/10.1016/j.conbuildmat.2015.07.006

[48] R. Demirboğa, İ. Türkmen, M.B. Karakoç, Relationship between ultrasonic velocity and compressive strength for high-volume mineral-admixtured concrete, Cement and Concrete Research 34(12) (2004) 2329-2336. https://doi.org/10.1016/j.cemconres.2004.04.017

[49] L.K. Bowlby, G.C. Saha, M.T. Afzal, Flexural strength behavior in pultruded GFRP composites reinforced with high specific-surface-area biochar particles synthesized via microwave pyrolysis, Composites Part A: Applied Science and Manufacturing 110 (2018) 190-196. https://doi.org/10.1016/j.compositesa.2018.05.003

[50] S.C. Chin, P.K. Gunasekaran, J. Che, N. Anand, J. Gimbun, Bamboo biochar and carbonation enhanced the compressive and flexural strength of cement mortar, Next Materials 9 (2025) 100959. https://doi.org/10.1016/j.nxmate.2025.100959

[51] M.G. Beltrán, A. Barbudo, F. Agrela, J.R. Jiménez, J. de Brito, Mechanical performance of bedding mortars made with olive biomass bottom ash, Construction and Building Materials 112 (2016) 699-707. https://doi.org/10.1016/j.conbuildmat.2016.02.065

[52] A.M. Neville, Properties of concrete, Longman London1995.

[53] M. Ghrici, S. Kenai, E. Meziane, Mechanical and durability properties of cement mortar with Algerian natural pozzolana, Journal of Materials Science 41(21) (2006) 6965-6972. https://doi.org/10.1007/s10853-006-0227-0

[54] M. Cyr, R. Idir, T. Poinot, Properties of inorganic polymer (geopolymer) mortars made of glass cullet, Journal of Materials Science 47(6) (2012) 2782-2797. https://doi.org/10.1007/s10853-011-6107-2

[55] S. Gupta, H.W. Kua, S.D. Pang, Biochar-mortar composite: Manufacturing, evaluation of physical properties and economic viability, Construction and Building Materials 167 (2018) 874-889. https://doi.org/10.1016/j.conbuildmat.2018.02.104

[56] Y. Jia, H. Li, X. He, P. Li, Z. Wang, Effect of biochar from municipal solid waste on mechanical and freeze–thaw properties of concrete, Construction and Building Materials 368 (2023) 130374. https://doi.org/10.1016/j.conbuildmat.2023.130374

[57] F. Bin Ahmed, K. Abid Ahsan, T. Shariff, S. Rahman Meem, Formulation of polynomial equation predicting the splitting tensile strength of concrete, Materials Today: Proceedings 38 (2021) 3269-3278. https://doi.org/10.1016/j.matpr.2020.10.017

[58] N. Arıoglu, Z.C. Girgin, E. Arıoglu, Evaluation of ratio between splitting tensile strength and compressive strength for concretes up to 120 MPa and its application in strength criterion, ACI materials journal 103(1) (2006) 18-24. https://doi.org/10.14359/15123

[59] ACI-318, Building Code Requirements for Structural Concrete and Commentary, American Concrete Institute, Farmington Hills, MI, 2022.

[60] G. Liao, D. Wang, W. Wang, Y. He, Microstructure, strength development mechanism, and CO2 emission analyses of alkali-activated fly ash-slag mortars, Journal of Cleaner

Production 442 (2024) 141116. https://doi.org/10.1016/j.jclepro.2024.141116

[61] I.P. Segura, T. Luukkonen, J. Yliniemi, H. Sreenivasan, A.J. Damø, L.S. Jensen, M. Canut, A.M. Kantola, V.-V. Telkki, P.A. Jensen, Comparison of One-Part and Two-Part Alkali-Activated Metakaolin and Blast Furnace Slag, Journal of Sustainable Metallurgy 8(4) (2022) 1816-1830. https://doi.org/10.1007/s40831-022-00606-9

[62] Q. Zhang, G. Ye, Dehydration kinetics of Portland cement paste at high temperature, Journal of Thermal Analysis and Calorimetry 110(1) (2012) 153-158. https://doi.org/10.1007/s10973-012-2303-9

[63] P. Chindasiriphan, H. Yokota, Y. Kawabata, P. Pimpakan, Combined effect of rice husk ash and superabsorbent polymer on self-healing capability of mortar, Construction and Building Materials 338 (2022) 127588. https://doi.org/10.1016/j.conbuildmat.2022.127588

[64] N. Vogler, P. Drabetzki, M. Lindemann, H.-C. Kühne, Description of the concrete carbonation process with adjusted depth-resolved thermogravimetric analysis, Journal of Thermal Analysis and Calorimetry 147(11) (2022) 6167-6180. https://doi.org/10.1007/s10973-021-10966-1

[65] S. Pilehvar, V.D. Cao, A.M. Szczotok, M. Carmona, L. Valentini, M. Lanzón, R. Pamies, A.-L. Kjøniksen, Physical and mechanical properties of fly ash and slag geopolymer concrete containing different types of micro-encapsulated phase change materials, Construction and Building Materials 173 (2018) 28-39. https://doi.org/10.1016/j.conbuildmat.2018.04.016

[66] T. Phoo-ngernkham, A. Maegawa, N. Mishima, S. Hatanaka, P. Chindaprasirt, Effects of sodium hydroxide and sodium silicate solutions on compressive and shear bond strengths of FA–GBFS geopolymer, Construction and Building Materials 91 (2015) 1-8. https://doi.org/10.1016/j.conbuildmat.2015.05.001

[67] A. Sabbah, S. Zhutovsky, The influence of clinkering conditions and cooling rate on the phase composition of Belite-Ye'elimite-Ferrite (BYF) clinker, Materials Today: Proceedings (2023). https://doi.org/10.1016/j.matpr.2023.06.097

[68] S. Kanchanasuta, N. Pisutpaisal, Waste utilization of palm oil decanter cake on biogas fermentation, International Journal of Hydrogen Energy 41(35) (2016) 15661-15666. https://doi.org/10.1016/j.ijhydene.2016.04.129

[69] A.G. Díaz, S. Bueno, L.P. Villarejo, D. Eliche-Quesada, Improved strength of alkali activated materials based on construction and demolition waste with addition of rice husk ash, Construction and Building Materials 413 (2024) 134823. https://doi.org/10.1016/j.conbuildmat.2023.134823

[70] M. Hossain, M. Karim, M. Elahi, M. Islam, M. Zain, Long-term durability properties of alkali-activated binders containing slag, fly ash, palm oil fuel ash and rice husk ash, Construction and Building Materials 251 (2020) 119094. https://doi.org/10.1016/j.conbuildmat.2020.119094

[71] R. De Michele, B. Liguori, D. Luceri, G. Zecca, A. Largo, C. Koidis, C. Achillas, A. Kalaitzidis, C. Pascale, C. Menna, Wood ash-based materials with improved post-fire resistance for building and infrastructure applications, Resources, Conservation and Recycling 222 (2025) 108475. https://doi.org/10.1016/j.resconrec.2025.108475

[72] O.J. Olatoyan, M.A. Kareem, A.U. Adebanjo, S.O.A. Olawale, K.T. Alao, Potential use of biomass ash as a sustainable alternative for fly ash in concrete production: A review, Hybrid Advances 4 (2023) 100076. https://doi.org/10.1016/j.hybadv.2023.100076

[73] X. Yu, J. Shi, Z. He, Ç. Yalçınkaya, V. Revilla-Cuesta, O. Gencel, Review of the materials composition and performance evolution of green alkali-activated cementitious materials, Clean Technologies and Environmental Policy 25(5) (2023) 1439-1459. https://doi.org/10.1007/s10098-023-02478-3

https://doi.org/10.12974/2311-8717.2025.13.16